Diffusion and localization of surface gravity waves over irregular bathymetry

A. Stepaniants*
Department of Civil and Environmental Engineering, Massachusetts Institute of Technology, Cambridge, Massachusetts 02139
(Received 29 March 2000; revised manuscript received 18 September 2000; published 21 February 2001)

An interaction of a linear surface gravity wave with weakly irregular one-dimensional bathymetry has been analyzed using the diagrammatic technique. The Boltzmann diffusion coefficient and the Anderson localization length for the wave energy density are expressed analytically via a correlation function of irregularities of the sea floor. The results are applied to different topographies. The effect of a finite region of irregularities, viscous damping, wave interaction, current, geometrically diffuse wave source, and anisotropy on localization is briefly discussed. The theory provides a scenario for the observation of large scale Anderson localization phenomenon in a tank or possibly in coastal waters.

DOI: 10.1103/PhysRevE.63.031202 PACS number(s): 05.60.Cd, 92.60.Dj, 94.10.Jd

I. INTRODUCTION

The behavior of surface gravity waves in near shore waters is of central importance to coastal oceanography and geomorphology. The interaction of waves with the coastal environment, such as bathymetry and the coastline, affects the climate waves as well as the evolution of the shoreline. Strong variations in near-shore topography can lead to significant attenuation or even total reflection of the waves.

For water wave propagation over regularly distributed sandbars on the bottom of the sea, Bragg resonance is known to produce forbidden frequency bands within which transmission is inhibited. This phenomenon is adapted to water waves from solid-state physics, where electron incident on the lattice, with energy in the forbidden bands, is completely reflected. For water waves over two-dimensional periodic bathymetry, Bragg resonance has been thoroughly studied by many authors. One of the first articles on this subject belongs to Davies (1982) [1], who demonstrated that resonant reflection takes place if the wavelength of the incident water wave is twice that of the bottom wavelength.

Unlike the case of periodic bathymetry, water wave propagating over irregularly distributed sandbars undergoes a series of elastic-scattering processes that lead to a randomization of its phase. As a result of this scattering, wave has a diffusive nature similar to a Brownian particle. What is more, at a large enough distance from the source, the wave intensity decays exponentially. Hence, the wave does not propagate beyond a certain region and is completely reflected. This phenomenon is also adopted from solid-state physics and is known as Anderson localization [2]. The important difference between Bragg scattering and Anderson localization phenomena is that the former occurs only for forbidden band frequency while the latter happens in the entire frequency range.

In solid-state physics, the phenomenon of Anderson localization of electrons is known to arise from interference of multiple-scattered electrons from impurities. It is attributed to the enhanced interference in the backscattering direction. This phenomenon is responsible for turning a one-dimensional (1D) or 2D conductor with a sufficient concentration of defects into an insulator at low temperatures. A self-consistent diagrammatic approach has been developed to describe the Anderson localization (for reviews the reader is referred to Refs. [3–6]) of electrons by impurities. This approach combines the Feynman diagrammatic technique for the Schroedinger wave equations with averaging over the impurity configurations and relies on the knowledge of the exact impurity scattering T matrix.

It is well understood that the concept of localization is very general and is not inherent to quantum particles only. The only two ingredients needed for the localization to take place are the wave equation and random media. There are numerous examples of classical wave localization, among which is the localization of visible light on concentrated suspension of microspheres [7], acoustic and electromagnetic wave localization [8], etc. One of the first attempts to study localization on the macroscopic scale has been made by Guazzelli *et al.*, (1983) [9] and later by Belzons *et al.* (1987) [10]. They observed the localization of 1D surface gravity waves in a tank in which the bottom was composed of random steps.

We present a theory that is similar to the self-consistent diagrammatic approach used for impurity scattering in the bulk. One of the differences is that a T matrix for scattering by an irregular bathymetry is not available. Another difference arises from averaging over the different configurations of the sea floor (as opposed to the positions of impurities). To resolve the first problem we perform canonical coordinate transformation that makes the boundaries flat. As a result of this transformation the boundary scattering problem transforms into the problem of scattering in the bulk. This approach to solving a stochastic boundary value problem is not new. For example, in Refs. [11,12] this method is applied to nanascale systems with rough boundaries. To overcome the second difference, we have developed an averaging technique for Feynman diagrams, which combined with the Born approximation from scattering theory significantly simplifies the diagrammatic derivation. This technique involves the expansion of averaged diagrams in deviation from Gaussian behavior. A similar expansion has been used together with

*Address for correspondence: Cold Spring Harbor Laboratory, 1 Bungtown Road, Freeman Building, Cold Spring Harbor, NY 11724. Email address: stephanya@cshl.org

the path integral method for sound propagation through a fluctuating environment in Refs. [13,14].

Since some near-shore topographies are very close to one dimensional we prefer to perform all the calculations for a 1D case. The approach presented can be easily extended to cover 2D situation. It is also very suitable for including the effects of weak wave interaction, current, and a mildly sloping irregular bathymetry.

This paper is organized as follows: The formulation of a problem of linear potential wave propagation over a 1D weakly irregular bathymetry is given in Sec. II. The canonical coordinate transformation reduces the scattering problem with the stochastic boundary condition to the scattering problem with irregularity in the bulk. In Sec. III, the latter problem is reformulated using the Green's function formalism and is solved by the Feynman diagrammatic approach in combination with averaging technique. Section IV contains the Boltzmann diffusion coefficient and Anderson localization length for the wave energy density that are expressed analytically via the correlation function of irregular topography. We do not go into a detailed derivation of these transport coefficients, but instead provide their expressions using general results from solid-state physics and kinetic theory. The results of Sec. IV are applied to random rough topography with the Gaussian correlation function and random step topography. Section V contains the comparison of our theory to the results of some theoretical and experimental publications on this subject. In Sec. VI, we list all limitations of the theory and review the possibility of water wave localization in coastal regions. The destructive effect of a finite region of irregularities (finite size effect), viscous damping, wave interaction, current, geometrically diffuse wave source, and anisotropy on localization phenomenon is discussed. Section VII is the conclusion.

II. FORMULATION OF THE PROBLEM

A. Linear potential theory

We consider a 1D linear potential wave propagating over an irregular bathymetry $\zeta(x)$. Function $\zeta(x)$ describes the deviation of water depth from its average value h. For simplicity we assume that the mean depth is horizontal, and $\langle\zeta(x)\rangle=0$ ($\langle\ldots\rangle$ denotes the configurational averaging). The velocity potential Φ for this system is described by the following equations [15]:

$$\begin{aligned}
&\frac{\partial^2\Phi}{\partial x^2}+\frac{\partial^2\Phi}{\partial z^2}=0, \quad -h+\zeta(x)\leqslant z\leqslant 0,\\
&\frac{\partial\Phi}{\partial z}-\zeta'(x)\frac{\partial\Phi}{\partial x}=0, \quad z=-h+\zeta(x),\\
&\frac{\partial^2\Phi}{\partial t^2}+g\frac{\partial\Phi}{\partial z}=0, \quad z=0,
\end{aligned} \tag{1}$$

the origin of the frame xz is chosen at the free surface with the coordinate z perpendicular to it, and g is the acceleration due to gravity. So far no assumption is made about the size of the bottom irregularities.

B. Coordinate transformation

The scattering problem (1) with the stochastic boundary condition at the bottom can be transformed into a problem with a flat boundary and irregularities in the bulk.

The canonical coordinate transformation must have the following characteristics:
(i) it would flatten the bottom boundary and leave the free surface of the water unperturbed;
(ii) the transformation would simplify the boundary condition at $z=-h+\zeta(x)$, getting rid of the term with $\zeta'(x)$, and leave the condition at $z=0$ unchanged;
(iii) the Jacobian of the transformation equals one.

The last condition is introduced for convenience, as it ensures the Hermiticity of the perturbation operator. Aside from these requirements the choice of the transformation is arbitrary (of course, the final result is the same for all different transformations).

The irregularities of the topography can be described by two characteristic lengths, the mean-square height l, and the correlation radius R. Our theory relies on the perturbation expansion, and is applicable only for small roughness

$$l\ll h,R. \tag{2}$$

This purely geometric condition is usually not very restrictive. Large irregularities of the bottom would lead to strong reflection or even trapping of the wave. This scenario is well beyond the scope of the diffusion or the Anderson localization phenomenon as we know it.

An example of a transformation that satisfies all of the above conditions, expanded to the first order in ζ is

$$\begin{aligned}
Z&=z+\left(2\frac{z^3}{h^3}+\frac{z^4}{h^4}\right)\zeta(x)-\left(\frac{z^3}{h^3}+\frac{z^4}{h^4}\right)\frac{h^2}{6}\zeta''(x)+O(\zeta^2),\\
X&=x+\left(6\frac{z^2}{h^2}+\frac{z^3}{h^3}\right)\int_0^x\zeta(t)dt\\
&\quad+\left(3\frac{z^2}{h^2}+4\frac{z^3}{h^3}\right)\frac{h}{6}\zeta'(x)+O(\zeta^2).
\end{aligned} \tag{3}$$

As a result of this transformation the scattering problem with the random boundary condition (1) transforms into a problem of scattering in the bulk

$$\begin{aligned}
&\left(\frac{\partial^2}{\partial X^2}+\frac{\partial^2}{\partial Z^2}-\hat{V}\right)\Phi=0, \quad -h\leqslant Z\leqslant 0,\\
&\frac{\partial\Phi}{\partial Z}=0, \quad Z=-h,\\
&\frac{\partial^2\Phi}{\partial t^2}+g\frac{\partial\Phi}{\partial Z}=0, \quad Z=0.
\end{aligned} \tag{4}$$

The perturbation operator $\hat{V}$ has the form (for brevity we use lower case x and z in what follows)

$$\hat{V}=\left[\frac{4}{h}\left(3\frac{z^2}{h^2}+2\frac{z^3}{h^3}\right)\zeta(x)-h\left(\frac{z^2}{h^2}+\frac{4}{3}\frac{z^3}{h^3}\right)\zeta''(x)\right]\left(\frac{\partial^2}{\partial x^2}-\frac{\partial^2}{\partial z^2}\right)$$
$$+\left[\frac{24}{h^2}\left(\frac{z}{h}+\frac{z^2}{h^2}\right)\int_0^x\zeta(x')dx'-2\left(\frac{z}{h}+2\frac{z^2}{h^2}+2\frac{z^3}{h^3}+\frac{z^4}{h^4}\right)\zeta'(x)+\frac{h^2}{3}\left(\frac{z^3}{h^3}+\frac{z^4}{h^4}\right)\zeta'''(x)\right]\frac{\partial^2}{\partial x\partial z}$$
$$+\left[\frac{12}{h^3}\left(1+2\frac{z}{h}\right)\int_0^x\zeta(x')dx'-\frac{1}{h}\left(1+4\frac{z}{h}-6\frac{z^2}{h^2}-4\frac{z^3}{h^3}\right)\zeta'(x)-h\left(\frac{1}{2}\frac{z^2}{h^2}+\frac{2}{3}\frac{z^3}{h^3}\right)\zeta'''(x)\right]\frac{\partial}{\partial x}$$
$$-\left[\frac{12}{h^2}\left(\frac{z}{h}+\frac{z^2}{h^2}\right)\zeta(x)-\left(\frac{z}{h}+2\frac{z^2}{h^2}-2\frac{z^3}{h^3}-\frac{z^4}{h^4}\right)\zeta''(x)-\frac{h^2}{6}\left(\frac{z^3}{h^3}+\frac{z^4}{h^4}\right)\zeta^{(4)}(x)\right]\frac{\partial}{\partial z}+O(\zeta^2). \quad (5)$$

The solution of the Eq. (4), that satisfies both boundary conditions at $z=-h$ and $z=0$, can be found in the form

$$\Phi(x,z,t)=\sum_{n=0}^{\infty}\int f_n(z,\omega)\phi_n(x,\omega)e^{i\omega t}\frac{d\omega}{2\pi}, \quad (6)$$

where functions f_n are orthonormal in the sense that

$$\int_{-h}^{0}f_n(z,\omega)f_m(z,\omega)dz=\delta_{n,m}. \quad (7)$$

Index $n=0$ denotes the propagating solution with

$$f_0(z,\omega)=\frac{\sqrt{2}\cosh[k_0(z+h)]}{[h+\sinh(k_0h)\cosh(k_0h)/k_0]^{1/2}}, \quad (8)$$

$$\omega^2=gk_0\tanh(k_0h). \quad (9)$$

The nonpropagating Evanescent modes correspond to $n=1$ to ∞

$$f_n(z,\omega)=\frac{\sqrt{2}\cos[k_n(z+h)]}{[h+\sin(k_nh)\cos(k_nh)/k_n]^{1/2}}, \quad (10)$$

$$\omega^2=-gk_n\tan(k_nh). \quad (11)$$

Substituting solution (6) into (4), and taking the Fourier transform we get

$$\sum_{n=0}^{\infty}\left(\frac{\partial^2}{\partial x^2}+(2\delta_{n,0}-1)k_n^2-\hat{V}(x,z)\right)f_n(z,\omega)\phi_n(x,\omega)=0, \quad -h\leqslant z\leqslant 0. \quad (12)$$

Multiplying this equation by $f_m(z,\omega)$ and integrating over z from $-h$ to 0 we obtain a system of coupled differential equations

$$\sum_{n=0}^{\infty}\left[\left(\frac{\partial^2}{\partial x^2}+(2\delta_{n,0}-1)k_n^2\right)\delta_{m,n}-\hat{V}_{m,n}(x)\right]\phi_n(x,\omega)=0. \quad (13)$$

The coupling is due to the nondiagonal nature of the random perturbation operator $\hat{V}$

$$\hat{V}_{m,n}=\int_{-h}^{0}f_m(z,\omega)\hat{V}f_n(z,\omega)dz. \quad (14)$$

III. DIAGRAMMATIC APPROACH

A. Green's function

The Green's function for the equations (13) is defined as the solution of the following set

$$\sum_{n=0}^{\infty}\left[\left(\frac{\partial^2}{\partial x^2}+(2\delta_{n,0}-1)k_n^2\right)\delta_{m,n}-\hat{V}_{m,n}(x)\right]G_{n,k}(x,x',\omega)=\delta_{m,k}\delta(x-x'). \quad (15)$$

To simplify the diagrammatic derivation it is useful to separate $\hat{V}$ into its average $\langle\hat{V}\rangle$ and the deviation from the average $\hat{V}-\langle\hat{V}\rangle$. The presence of $\langle\hat{V}\rangle=O(\zeta^2)$, under the condition (2) leads to a mean-field correction to the dispersion relation, and small coupling between the Eq. (15) already in the zero order in $\hat{V}-\langle\hat{V}\rangle$. The goal of this paper is to calculate attenuation of the wave to the leading order (not the mean-field corrections to the dispersion relation and transport coefficients) that comes from the term $\hat{V}-\langle\hat{V}\rangle$. For this reason we can truncate the expression of $\hat{V}$ (5) at the leading order $O(\zeta)$. In all the following calculations we will use this truncated operator, that has zero average due to the random nature of irregular topography.

In the zero order in perturbation $\hat{V}$ the set of Eq. (15) decouples and the solution is easily found in Fourier space,

$$G_{n,k}^{(0)R,A}(x-x',\omega)=\int G_{n,k}^{(0)R,A}(k,\omega)e^{ik(x-x')}\frac{dk}{2\pi},$$
$$G_{n,k}^{(0)R,A}(k,\omega)=\delta_{n,k}G_n^{(0)R,A}(k,\omega), \quad (16)$$
$$G_n^{(0)R,A}(k,\omega)=\frac{1}{(2\delta_{n,0}-1)k_n^2(\omega)-k^2\mp i0}. \quad (17)$$

Superscripts R and A stand for retarded and advanced Green's functions, and a small pole $i0$ in the denominator

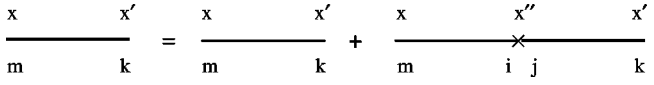

FIG. 1. Diagrammatic representation of the Eq. (18) for the Green's function $G^{R,A}$.

specifies the direction of contour integration for $G_0^{(0)R,A}$ in Eq. (16). The nonperturbed Green's functions corresponding to Evanescent modes ($n=1$ to ∞) attenuate exponentially at distances between the observer x and the source x' larger than the wavelength λ. For these modes small pole $i0$ is not important, and there is no difference between retarded and advanced Green's functions.

The exact solution of the set of equations (15) (exact Green's function) $G_{m,k}^{R,A}(x,x',\omega)$ satisfies the integral equation

$$G_{m,k}^{R,A}(x,x',\omega)=G_{m,k}^{(0)R,A}(x-x',\omega)+\sum_{i,j=0}^{\infty}\int G_{m,i}^{(0)R,A}(x-x'',\omega)\times\hat{V}_{i,j}(x'',\omega)G_{j,k}^{R,A}(x'',x',\omega)dx''. \quad (18)$$

The expression (18) is illustrated in Fig. 1 using Feynman diagrams in coordinate representation. The thin line denotes the nonperturbed Green's function $G^{(0)R,A}$, the thick line corresponds to the exact $G^{R,A}$, and the cross is the perturbation $\hat{V}$. Over all internal indexes (i,j) and variables (x'') summation and integration is assumed.

B. Averaging technique

We define a many point correlation ξ_n of a random function A as the average over all realizations of the product

$$\xi_n(x_1,x_2,\ldots,x_n)=\langle A(x_1)A(x_2)\ldots A(x_n)\rangle. \quad (19)$$

Let us assume that a random function $A(x)$ has the following properties:

(i) the even point correlation function ξ_{2n} of A is translationally invariant

$$\xi_{2n}(x_1,x_2,\ldots,x_{2n})=\xi_{2n}(x_1+a,x_2+a,\ldots,x_{2n}+a) \quad (20)$$

(ii) for an odd number of points the correlation function ξ_{2n+1} is zero

$$\xi_{2n+1}(x_1,x_2,\ldots,x_{2n+1})=0 \quad (21)$$

(iii) for two groups of points $x_1,\ldots,x_k$ and $x_{k+1},\ldots,x_{2n}$, separated by a distance much greater than the correlation radius R of random function $A(x)$, the $2n$-point correlation function decouples

$$\xi_{2n}(x_1,\ldots,x_{2n})=\xi_k(x_1,\ldots,x_k)\xi_{2n-k}(x_{k+1},\ldots,x_{2n}). \quad (22)$$

If $A(x_1),A(x_2),\ldots,A(x_{2n})$ are drawn from a Gaussian distribution the $2n$-point correlation function completely decouples into a sum of all possible products of two-point correlation functions

$$\xi_{2n}^G(x_1,\ldots,x_{2n})=\sum_P \xi_2^G(x_{i_1},x_{i_2})\xi_2^G(x_{i_3},x_{i_4})\ldots\xi_2^G(x_{i_{2n-1}},x_{i_{2n}}), \quad (23)$$

where the summation goes over all possible permutations of points $x_1,x_2,\ldots,x_{2n}$.

For function A (not necessarily Gaussian) satisfying the conditions (20), (21), and (22) we recursively define a deviation of the $2n$-point correlation function from its Gaussian analog

$$D_{2n}(x_1,\ldots,x_{2n})=\xi_{2n}(x_1,\ldots,x_{2n})-\sum_P \xi_2(x_{i_1},x_{i_2})\ldots\xi_2(x_{i_{2n-1}},x_{i_{2n}})-\sum_{j=1}^{n-1}\sum_P D_{2j}(x_{i_1},\ldots,x_{i_{2j}})\times\xi_{2(n-j)}(x_{i_{2(j+1)}},\ldots,x_{i_{2n}}). \quad (24)$$

It follows from Eq. (24) that $D_2=0$. Another important property of the deviation $D_{2n}(x_1,\ldots,x_{2n})$ is that it is translationally invariant satisfying the condition (20), and it goes to zero as the distance between any two groups of its variables becomes larger than the correlation radius R [in contrast to the $2n$-point correlation function ξ_{2n}, which decouples according to Eq. (22)]. This property of D_{2n}, which follows from Eq. (22), will be used later in combination with the Born approximation to simplify the evaluation of the average Green's function.

C. Average Green's function

The configurationally averaged Green's function $\langle G_{m,k}^{R,A}\rangle$ depends on the difference between the coordinates of the source and the observer, and can be found from perturbative expansion of the right-hand side of the Eq. (18). It contains the averages of products of random perturbation $\hat{V}$, which is assumed to meet all the conditions of Sec. III B. From this moment it is more convenient to continue the derivation in k space.

After we reduce all the different products of random perturbation $\hat{V}$ according to Eq. (24), the resulting averages can be described by averaged Feynman diagrams. Some of these diagrams are presented in Fig. 2. The shaded line in the left-hand side corresponds to the average Green's function $\langle G_{m,n}^{R,A}(k,\omega)\rangle$, the thin line again is $G^{(0)R,A}(k,\omega)$. The dashed (averaging) line represents the configurational averaging. Hence, in the second diagram on the right of the equality sign two crosses connected by a dashed line denote $\langle V_{i,j}(k,k_1)V_{p,q}(k_1,k)\rangle$, where

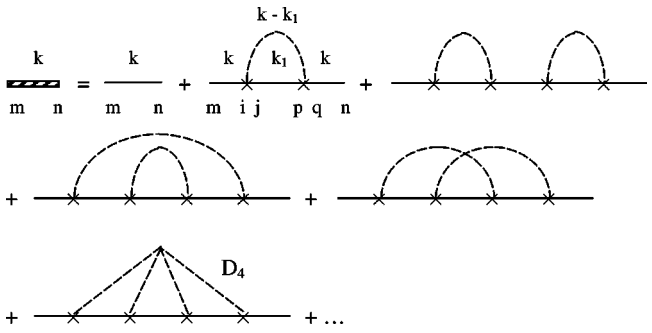

FIG. 2. Diagrammatic expansion of the average Green's function $\langle G^{R,A}(k,\omega)\rangle$.

$$V_{i,j}(k,k_1)=\int e^{-ikx}\hat{V}_{i,j}(x)e^{ik_1x}dx. \tag{25}$$

The averaging lines connecting several crosses (last diagram) represent the deviation of the many point correlation function from its Gaussian analog $D_{2n}(k-k_1,k_1-k_2,\ldots,k_{2n-1}-k)$. At every cross (intersection of two thin lines and an averaging line) there is a conservation of the wave number (see the second diagram on the right-hand side of the equation in Fig. 2).

To provide a better understanding of these pictures we put the second diagram in the right-hand side of the equality sign in Fig. 2 in the algebraic form

$$\sum_{i,j,p,q} G^{(0)R,A}_{m,i}(k,\omega)G^{(0)R,A}_{q,n}(k,\omega) \times\int G^{(0)R,A}_{j,p}(k_1,\omega)\langle V_{i,j}(k,k_1)V_{p,q}(k_1,k)\rangle\frac{dk_1}{2\pi}.$$

Figure 2 contains a diagrammatic expansion of the average Green's function in terms of a small perturbation $\hat{V}$. This expansion involves an infinite number of terms. We can reduce the number of terms in this expansion (still leaving an infinite number) by introducing a Σ matrix. This procedure will account for all the diagrams that can be cut in two by a vertical line intercepting only a Green's function. Diagrams of this kind are called reducible diagrams (third diagram on the right of the equality sign, Fig. 2). The result is known as Dyson equation and is illustrated in Fig. 3.

In algebraic form Dyson equation is

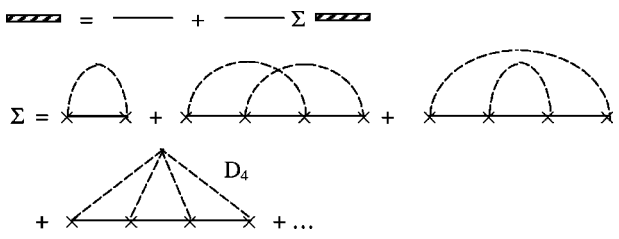

FIG. 3. Dyson equation and diagrammatic expansion of the Σ matrix.

$$\langle G^{R,A}_{m,n}(k,\omega)\rangle=\sum_{i,j} G^{(0)R,A}_{m,i}(k,\omega)\Sigma^{R,A}_{i,j}(k,\omega)\langle G^{R,A}_{j,n}(k,\omega)\rangle. \tag{26}$$

Solving this matrix equation we find the average Green's function $\langle G^{R,A}_{m,n}(k,\omega)\rangle$

$$\langle \mathbf{G}^{R,A}(k,\omega)\rangle=[\mathbf{G}^{(0)}(k,\omega)^{-1}-\mathbf{\Sigma}^{R,A}(k,\omega)]^{-1}, \tag{27}$$

where bold letters represent matrixes, and -1 in the superscript denotes the matrix inversion. At this point in the diagrammatic derivation, wave scattering by random irregularities of the sea floor converges with the well-established theory of electron impurity scattering.

D. Born approximation and mean-free-path

Up to this moment we did not make any assumptions on the wavelength λ. The assumption (2) is purely geometric. To find the average Green's function according to Eq. (27) it is necessary to make an approximation of the Σ matrix, given by the diagrammatic expansion in Fig. 3. The approximation of the Σ matrix in the leading order (leaving only the first diagram in Fig. 3) comes from scattering theory and is called the Born approximation. This approximation for scattering by impurities simply means that a particle (wave) undergoes two (if one uses the coherent potential approximation) consecutive scattering by one impurity before it is scattered by another impurity.

For scattering by an inhomogeneous topography the picture is similar. In this case, the Born approximation means that a wave propagating freely from the source, is scattered twice in the vicinity of the same irregularity (defined by the correlation radius R of the topography) and propagates freely to the next irregularity where it again undergoes a double scattering, and so on until it reaches the observer. The Born approximation implies that scattering is weak, and there is no need to account for multiple (more than double) scattering processes by the same irregularity.

Comparing the fourth-order diagrams in the expansion for the Σ matrix given in Fig. 3 to the diagram of the second order in $\hat{V}$ (the leading diagram in the expansion) we get the Born approximation condition

$$\left(\frac{lR}{h^2}\right)^2 \ll\left[\max\left(kh,\frac{1}{kh}\right)\right]^2. \tag{28}$$

The diagrams containing the deviation D are smaller than the diagrams of the same order not involving D. In proving this statement one has to take advantage of the property of D_{2n}, that it goes to zero as the distance between any two groups of its variables becomes larger than the correlation radius R, setting a constrain on the integration region. This insures that the Σ matrix can be correctly approximated by the first expansion diagram in Fig. 3.

It is worth mentioning that if $(lR/h^2)^2 \ll 1$, the Born approximation condition (28) is satisfied for all waves.

The Born approximation simplifies the matrix inversion in the expression for the Green's function (27). For weak perturbation, the nondiagonal elements in Eq. (27) are small, and $\langle G \rangle$ can be approximated as

$$\langle G^{R,A}_{i,j}(k,\omega)\rangle = \frac{\delta_{i,j}}{(2\delta_{i,0}-1)k_i^2(\omega)-k^2-\Sigma^{R,A}_{i,i}(k,\omega)}. \tag{29}$$

The propagating Green's function in this approximation is not coupled to the Evanescent (nonpropagating) modes, and has a form

$$\langle G^{R,A}_{0,0}(k,\omega)\rangle = \frac{1}{k_0^2(\omega)-k^2-\Sigma^{R,A}_{0,0}(\omega)}. \tag{30}$$

The Born approximation (28) also insures that the imaginer part of $\Sigma^{R,A}_{0,0}(\omega)$ is much smaller than $k_0^2(\omega)$, and the thickness of the spectrum line is negligible

$$\langle G^{R}_{0,0}(k,\omega)\rangle - \langle G^{A}_{0,0}(k,\omega)\rangle = 2\pi i\,\delta(k_0^2(\omega)-k^2). \tag{31}$$

The Σ matrix in the Born approximation (first expansion diagram for Σ in Fig. 3) can be calculated according to the rules of the diagrammatic technique. $\Sigma^R_{0,0}$ and $\Sigma^A_{0,0}$ are complex conjugate to each other, and their difference describes the attenuation of the average wave amplitude due to scattering,

$$\begin{aligned}\Sigma^R_{0,0}(\omega)-\Sigma^A_{0,0}(\omega) &= \int U_0(k_0,k')[\langle G^R_{0,0}(k',\omega)\rangle \\ &\quad - \langle G^A_{0,0}(k',\omega)\rangle]\frac{dk'}{2\pi} \\ &= \frac{i}{2k_0}[U_0(k_0,k_0)+U_0(k_0,-k_0)],\end{aligned} \tag{32}$$

where we used Eq. (31) to evaluate the integral. Hear U_0 represents two crosses connected by an averaging line and is called the Boltzmann irreducible vertex function,

$$U_0(k,k') = \langle V_{0,0}(k,k')V_{0,0}(k',k)\rangle. \tag{33}$$

Direct calculations for the perturbation operator (5) give the following expression for the irreducible vertex function U_0 and $\mathrm{Im}[\Sigma^R] = -\mathrm{Im}[\Sigma^A]$

$$U_0(k,k') = \left[2kk' + (k+k')^2\left(\frac{1}{2} + \frac{3\sinh(2kh)}{4k^3h^3} + \frac{3[1-\cosh(2kh)]}{4k^4h^4}\right)\right]^2 \frac{\xi_2(k'-k)}{[h+\sinh(2kh)/2k]^2}, \tag{34}$$

$$\begin{aligned}&\mathrm{Im}\,[\Sigma^R(\omega)] \\ &= \left[\xi_2(2k_0) + \xi_2(0)\left(2 + \frac{3\sinh(2k_0h)}{2k_0^3h^3} + \frac{3[1-\cosh(2k_0h)]}{2k_0^4h^4}\right)^2\right]\frac{k_0^3}{[h+\sinh(2k_0h)/2k_0]^2}.\end{aligned} \tag{35}$$

In Eq. (34) $|k| = |k'| = k_0$.

The mean-free-path l_{mfp}, i.e., the distance over which waves lose coherence, is defined as

$$l_{mfp}(\omega) = \frac{2k_0(\omega)}{\mathrm{Im}[\Sigma^R_{0,0}(\omega)-\Sigma^A_{0,0}(\omega)]}. \tag{36}$$

It follows from Eq. (30) that the average wave amplitude decays exponentially with the exponent $1/2l_{mfp}(\omega)$, and

$$\begin{aligned}&l_{mfp}(\omega)^{-1} \\ &= \left[\xi_2(2k_0) + \xi_2(0)\left(2 + \frac{3\sinh(2k_0h)}{2k_0^3h^3} + \frac{3[1-\cosh(2k_0h)]}{2k_0^4h^4}\right)^2\right]\frac{k_0^2}{[h+\sinh(2k_0h)/2k_0]^2}.\end{aligned} \tag{37}$$

IV. RESULTS

A. Diffusion coefficient and localization length

In this section we use some general results of solid-state physics and kinetic theory to obtain analytic expressions of the Boltzmann transport equation, Boltzmann diffusion coefficient, and the localization length for the wave energy density. We are not going to duplicate the derivation of equations from this theories. For a detailed diagrammatic description of transport phenomena we refer the reader to numerous books and reviews [4,5,16,3,6].

Wave energy (energy per unit area of the sea surface) which is the sum of the kinetic and potential energies can be defined in terms of the velocity potential in the following way [15]

$$E(x,t) = \frac{\rho}{2}\int_{-h}^{0}\left(\left|\frac{\partial\Phi}{\partial x}\right|^2 + \left|\frac{\partial\Phi}{\partial z}\right|^2\right)dz + \frac{\rho}{2g}\left|\frac{\partial\Phi}{\partial t}\right|^2_{z=0}. \tag{38}$$

The energy stored in the propagating mode $(n=0)$, averaged over several typical periods of waves from the incident

band, can be found by substituting the velocity potential in the form of Eq. (6) into the above expression and using the orthonormality condition (7),

$$E_{0,0}(x,t)=\frac{\rho}{2}\int\left\langle\left|\frac{d\phi_0}{dx}\right|^2+k_0^2(\omega)\left|\phi_0\right|^2\right\rangle\frac{d\omega}{2\pi}. \tag{39}$$

Averaging Eq. (39) over different configurations of the sea floor we obtain the expression for the wave energy density

$$E_{0,0}(\omega,x,t)=\frac{\rho}{2}\left(\left\langle\left|\frac{d\phi_0}{dx}\right|^2\right\rangle+k_0^2(\omega)\langle|\phi_0|^2\rangle\right). \tag{40}$$

This expression is identical to the one for electrons in disordered media, described by the Schroedinger equation. Hence, the results from solid-state physics can be used to find the transport free path, the Boltzmann diffusion coefficient, and the localization length for wave energy density.

The transport free path l_{mfp}^{tr}, the length scale over which the wave energy density becomes diffuse, is

$$l_{mfp}^{tr}(\omega)=\frac{2k_0^2}{U_0(k_0,-k_0)}=\frac{[h+\sinh(2k_0h)/2k_0]^2}{2k_0^2\xi_2(2k_0)}. \tag{41}$$

The 1D Boltzmann diffusion coefficient D_B is related to l_{mfp}^{tr}

$$D_B(\omega)=C_g(k_0)l_{mfp}^{tr}(\omega)=\frac{C_g(|k_0|)[h+\sinh(2k_0h)/2k_0]^2}{2k_0^2\xi_2(2k_0)}, \tag{42}$$

where $C_g(k_0)=d\omega/dk_0$ is the group velocity of the wave.

In the 1D case a coherent back scattering (interference of waves in a back scattered direction) leads to the reduction of the diffusion coefficient (42) and localization. To describe this effect one has to go beyond the Boltzmann approximation, and consider a series of maximally crossed diagrams in the irreducible vertex function $U_0(k,k')$ [the Boltzmann approximation includes only one diagram (33)]. The result of the 1D localization theory is that the wave energy density decays exponentially with the distance from the source to the observer, and the exponent is $2/l_{loc}$,

$$l_{loc}(\omega)=4l_{mfp}^{tr}(\omega)=\frac{2[h+\sinh(2k_0h)/2k_0]^2}{k_0^2\xi_2(2k_0)}. \tag{43}$$

To summarize, the behavior of the wave energy density has a different nature depending on the distance between the source and observer. At a small propagation distance (smaller than the transport free path, but much larger than the typical wavelength) the wave energy density propagates according to the Boltzmann transport equation

$$\frac{\partial}{\partial t}E_{0,0}(k_0,x,t)+C_g(k_0)\frac{\partial}{\partial x}E_{0,0}(k_0,x,t)=\frac{\pi C_g(k_0)}{k_0}\int U_0(k_0,k)\,\delta(k^2-k_0^2)\times[E_{0,0}(k,x,t)-E_{0,0}(k_0,x,t)]\frac{dk}{2\pi}, \tag{44}$$

where $E_{0,0}(k_0,x,t)$ is the wave energy density stored in the propagating mode corresponding to the wave frequency ω [ω is related to k_0 according to Eq. (9)]. At an intermediate propagation distance (order of the transport free path but smaller than the localization length l_{loc}) the wave energy density propagation is diffusive. In 1D the interval when diffusion can occur is very narrow, and the Boltzmann diffusion coefficient (42) is renormalized down by the coherent back scattering phenomenon. At large distance (larger than the localization length) there is no transport or diffusion, and the wave energy density is localized.

B. Correlation function of irregular topography

In this section we consider two possible realizations of the irregular topography. The results for the transport free path (41) and the Boltzmann diffusion coefficient (42) are related to the localization length, and in what follows we will show plots only for the localization length (43).

For some random topographies the two point correlation function can be approximated by a Gaussian

$$\xi_2(x)=l^2\exp(-x^2/2R^2),\qquad \xi_2(k)=\sqrt{2\pi}l^2R\exp(-k^2R^2/2). \tag{45}$$

In these expressions l is the mean-square average height of the irregularities and R is the correlation radius (characteristic size). The second expression in Eq. (45) is the correlation function in the Fourier representation.

Figure 4 shows the dependence of the localization length (43) on wave number k_0 for the Gaussian correlation (45). This dependence has some general features inherent to all correlation functions of bottom irregularities. The localization length diverges at very small and very large frequencies. In the low-frequency limit (Rayleigh scattering) the waves do not resolve the structure of the irregularities, the scattering cross section in general is proportional to ω^4, and the transport free path diverges as $k^2\omega^{-4}\sim k^{-2}$. In the high-frequency limit the localization length diverges again, because the points of two consecutive scattering processes are not correlated. Another obvious feature of the localization length is that it increases with the increase in depth h (see Fig. 4). The minimal localization length corresponds to $kR\sim 1$, when scattering is the strongest.

Next, we consider the topography consisting of random steps. The lengths of the steps L_i are randomly drawn from the distribution uniform on $L-\Delta L$ to $L+\Delta L$. The heights of the steps H_i above the average depth level are drawn from the distribution uniform on the interval from $-\Delta H$ to ΔH,

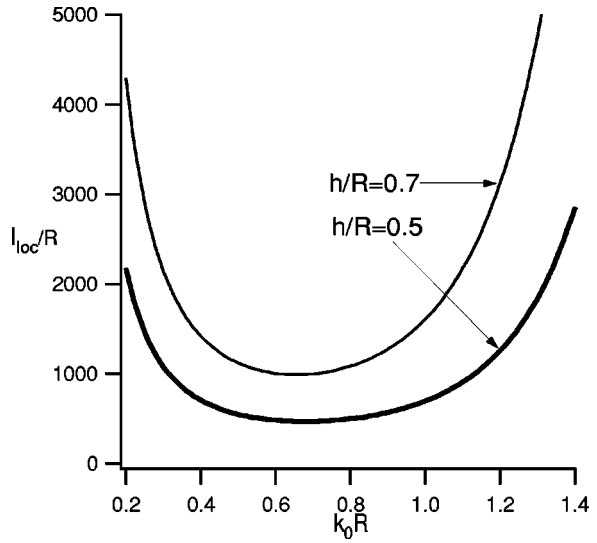

FIG. 4. Localization length l_{loc}/R, Eq. (43) as a function of wave number k_0R for the Gaussian correlation function of irregular topography (45) with $l/R=0.1$. The thick line corresponds to $h/R=0.5$, and the thin line to $h/R=0.7$.

$$\zeta(x)=\sum_{-\infty}^{+\infty} H_i[\,\theta(x-x_{i-1})-\theta(x-x_i)\,],$$
$$L_i=x_i-x_{i-1}. \tag{46}$$

The correlation function for this topography is

$$\xi_2(x)=\frac{\Delta H^2}{3L}\times\begin{cases} L-|x|, & |x|\leqslant L-\Delta L \\ (L+\Delta L-|x|)^2/4\Delta L, & L-\Delta L<|x|\leqslant L+\Delta L \\ 0, & L+\Delta L<|x|, \end{cases}$$

$$\xi_2(k)=\frac{2\Delta H^2}{3Lk^2}\left(1-\frac{\sin(k\Delta L)}{k\Delta L}\cos(kL)\right). \tag{47}$$

The correlation radius R in this case is of the order of L, and the mean-square height of the irregularities $l=\Delta H/\sqrt{3}$.

This geometry is considered in order to compare the results of this theory to the experimental work of Guazzelli *et al.*, Belzons *et al.*, and some theoretical calculations. This is done in the next section.

Finally, let us see what happens if we formally apply the result (43) to a regular, periodic bathymetry with the period $2\pi/K$,

$$\zeta(x)=H\cos(Kx). \tag{48}$$

The correlation function in this case is

$$\xi_2(x)=\frac{H^2}{2}\cos(Kx),$$
$$\xi_2(k)=\frac{\pi H^2}{2}[\,\delta(K+k)+\delta(K-k)\,], \tag{49}$$

and the correlation radius R is infinite. The infinite correlation radius immediately violates the Born approximation condition (28). In spite of this, the localization length calculated according to the equations (43) and (49) has a very interesting feature. The localization length for the periodic bottom is infinite (wave propagates freely) for all wave numbers k except for $k=K/2$ when the localization length becomes zero (no propagation). This is a trace of the Bragg resonance. The reason why we obtain only the indication of the first forbidden band can be explained by the fact that the Boltzmann approximation, used in the derivation, is only the second-order approximation to the Σ matrix.

V. COMPARISON WITH OTHER CALCULATIONS

In this section, we compare the results of our theory to some theoretical and experimental works on 1D water wave localization over irregular bathymetry. We start with the experimental work of Belzons *et al.* [10]. One of the results of this paper is the dependence of the localization length on the wave frequency. The measurements were done in the tank in which the bottom was composed of 58 random steps. Due to the finite-size effect the error bars of the measurements were very large everywhere, except for the frequencies for which the localization is the strongest. The error bars are the result of configurational averaging over five different realizations of the bottom geometry. The work of Guazzelli *et al.* [9], which is the first experimental work on surface gravity wave localization, is done for a single configuration and does not include error bars. For this reason it is not well suited for comparison.

In Fig. 5, we compare the results of our theory [Eqs. (43) and (47)] with the experimental results of Belzons *et al.* The agreement between theory and the experiment is very good in spite of the fact that the mean-square average height for the steps $l=0.72$ cm, and it is not much smaller than $h=1.25$ cm, violating the perturbation condition (2). This can be explained by the fact that the next correcting term to the localization length provided by Eq. (43) is of the order of $l^2/h^2=0.33$, and is small in comparison to the leading term. Since the experiment has been done in 1 Hz to 3 Hz frequency range, the Born approximation (28) is valid.

There are two inherent problems in comparing the results of the experiment to the theoretical results obtained from the linear potential theory. The steps in the experiment of Belzons *et al.* dissipate energy by generating vortices around the edges. It is very difficult to distinguish the localization related decrease in the average wave amplitude from the above dissipation mechanism. Another problem is associated with very high steps (steps that almost reach the free surface of the water). In order to make an experiment in a relatively small tank, and to have reasonably small localization length (smaller than the size of the tank) the authors had to use tall steps. For waves over these steps the linear theory is not valid, and instead of Anderson localization one could get nonlinear trapping of the wave.

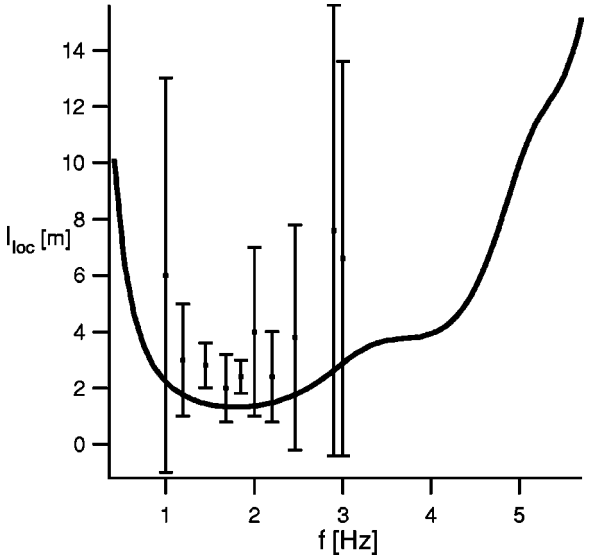

FIG. 5. Localization length l_{loc} as a function of wave frequency f for an irregular topography composed of random steps. The solid line is the result for the infinite geometry provided by the Eqs. (43) and (47). The points with error bars are the experimental results of Belzons *et al.* [10]. The average water depth is $h=1.25$ cm, the average length of the step is $L=4.1$ cm, $\Delta L=2.0$ cm, and $\Delta H=1.25$ cm.

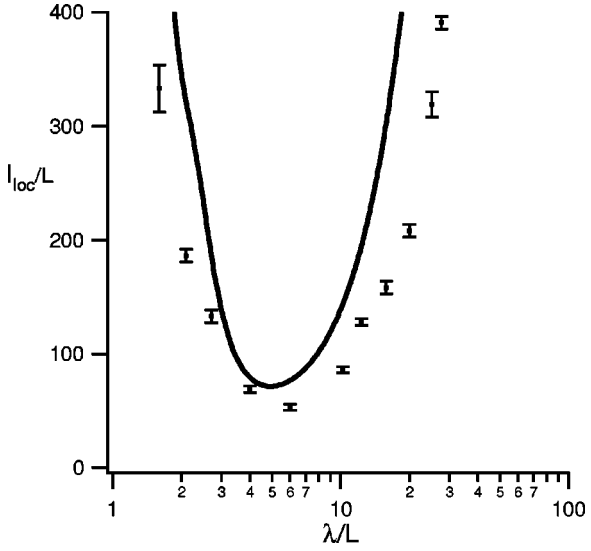

FIG. 6. Localization length l_{loc}/L as a function of wavelength λ/L for an irregular topography composed of random steps. The solid line is the result provided by the Eqs. (43) and (47). Points with error bars are the numerical calculation of Devillard *et al.*, Ref. [17], where $\Delta L/L=0.5$, $\Delta H/h=5/7$, and $h/L=7/16$.

In the theoretical work of Devillard *et al.* [17], the localization length is found from the linear potential shallow water theory. The authors are using the transfer-matrix approach for the bottom composed of random steps. This 1D theory does not provide correct results in the limit of high wave numbers k, due to the fact that the shallow water theory condition $kh \ll 1$ breaks down. Otherwise, the results agree with our calculations done for steps with small amplitudes. To extend the theory to the large k region, the authors perform a numerical study based on the full linear potential theory. A wide spacing assumption $R \gg h$ is made in order to neglect the coupling to the nonpropagating Evanescent modes.

Figure 6 demonstrates a qualitative agreement between the results of our theory (43), (47) (solid line), and the numerical calculation of Devillard *et al.* [17], (points with error bars). The perturbation condition (2), and the Born approximation (28) for this case are not thoroughly satisfied.

Nachbin [18] provides a 1D shallow water localization theory for an arbitrary amplitude rapidly varying topography with $kR \ll 1$ and $kh \ll 1$. This theory is based on the conformal mapping of the rough channel into a channel with a flat bottom (similar to our approach for small roughness). The localization results, in the limit of a small amplitude of variations of the topography, coincide with a limit of Eq. (43) for small k.

In contrast to the above theoretical works on 1D localization, our theory for small size irregularities (2) and (28) is valid for arbitrary irregular geometry (the transfer-matrix approach is applicable for steps only) and for a very large range of wave numbers k. Another advantage of the theory is that it can be easily modified to include a 2D case. Since irregularities of the near-shore ocean floor are usually small, and conditions (2) and (28) are valid for many coastal regions, this approach is well suited for investigating the possibility of a large scale Anderson localization phenomenon.

VI. LIMITATION OF THE THEORY AND POSSIBILITY OF OBSERVATION OF WATER WAVE LOCALIZATION

In this section, we briefly discuss the assumptions made in the theory on the nature of the wave and the environment in order to have localization according to Eq. (43). The assumptions a through f are needed for a tank experiment similar to the one done by Belzons *et al.* [10]. For a near-shore localization extra assumptions g, h, and i are necessary.

(a) Linear potential flow: The main restriction of the presented theory is the assumption of a linear potential flow, that is a limitation on the wave amplitude a [15],

$$ak_0 \ll 1, \quad \frac{a}{h} \ll 1, \quad \frac{a}{k_0^2 h^3} \ll 1. \tag{50}$$

(b) Wave interaction: It is well known [15], that small wave interaction leads to the nonlinear Schroedinger equation, and that the effect of nonlinearity becomes important over propagation distance that scales with wave amplitude as a^{-2}. We consider propagation distance of the order of the transport free path or the localization length, that scale with the amplitude of the irregular topography as l^{-2}. Hence, for small waves $a<l$, wave energy density transport and localization will not be affected by nonlinearity.

(c) Small inhomogeneities: The next limitation of the theory is the geometric condition (2). We assumed that the mean-square height of the irregularities of the topography is small.

(d) The Born approximation: The Born approximation limits the theory to a certain range of wave numbers k_0 according

to Eq. (28). This approximation for weakly irregular bathymetry is usually not very restrictive. If $(lR/h^2)^2 \ll 1$ the Born approximation is valid for all waves.

(e) Viscous damping: In the presence of viscosity ν the wave amplitude decays exponentially, with dissipation length $d(\omega)$. For weakly irregular bathymetry (2) the dissipation length $d(\omega)$ can be approximated as that for the wave propagating over a constant depth [15],

$$d(\omega) = \frac{C_g(k_0)\sinh(2k_0h)}{2\nu k_0^2 \sinh(2k_0h) + k_0(\nu\omega/2)}. \tag{51}$$

Since both the dissipation and the localization processes are exponential, small dissipation length $d(\omega)$ would mask the localization phenomenon completely. Hence, it is important for the observation of the water wave localization that the dissipation length is larger than the localization length (43). The kinematic viscosity for water is small, $\nu \approx 0.01$ cm/s, and the dissipation length (51) for waves with the strongest interaction with irregular bathymetry $k_0R \sim 1$ is usually much larger than the localization length.

(f) Finite-size effect: The described theory was derived for infinite irregular geometry. In reality, the results are valid for regions of the order or larger than the localization length. For smaller regions the finite-size effects become very important, destroying localization and resulting in the large uncertainty in the reflection coefficient [3].

(g) Geometrically diffuse wave source: It was assumed in the derivation that the incident wave is monochromatic and originates from a single source. In reality, the sources of ocean waves are geometrically diffuse and waves from these sources travel in wave packets (no interference between packets is considered). The finite size of a wave packet $\mathcal{L}$ leads to the uncertainty in the wave number k_0, that is of the order of $\delta k \sim 1/\mathcal{L}$. The localization length is not affected by this uncertainty if δk does not modify the imaginary part of the pole in the Green's function (27), $k_0\delta k \ll \mathrm{Im}[\Sigma(\omega)] \sim k_0/l_{loc}$. Or, the size of the wave packet has to be larger than the localization length $\mathcal{L} \gg l_{loc}$. This condition is similar to f (finite-size effect), and one should expect the smaller size wave packets to lead to large uncertainties in localization length.

(h) Current: Localization is the consequence of the wave interference in the back scattered direction. Even a small current can destroy the phase coherence of the interfering waves. The current U should be sufficiently small, so that the wave that travels a distance of the order of the localization length and comes back to the original point in the course of numerous scattering processes, would gain an insignificant phase shift

$$\frac{l_{loc}(\omega)k_0^2U}{\omega} \ll 1. \tag{52}$$

(i) Anisotropy: It is known that in an isotropic 2D situation the localization length is exponentially large, and localization effects are weak [3]. There is a critical amount of anisotropy (large anisotropy) when one can treat a 2D system as one dimensional. In a near-shore region, irregularities of the topography (sandbars) are mostly oriented parallel to the shoreline, or their correlation radius in the direction parallel to the shore is much larger than the one in the perpendicular direction, $R_\parallel \gg R_\perp \equiv R$. The difference in directions of incident and scattered waves (in the course of a single scattering process) due to this large anisotropy is of the order of $R_\perp/R_\parallel \ll 1$. Consequently, the phase shift due to the anisotropy is of the order of $(R_\perp/R_\parallel)^2$. This phase difference will accumulate in the process of multiple scattering. In the region of size l_{loc} the number of scattering processes is of the order of $l_{loc}/R_\perp$, and the overall phase shift is $(R_\perp/R_\parallel)^2 l_{loc}/R_\perp$. If this phase shift is small, or $R_\parallel \gg \sqrt{R_\perp l_{loc}}$, the results of 1D theory can be applied to anisotropic 2D geometry.

In general, the assumptions a–f that are sufficient for a tank experiment are not very restrictive, and can be easily met for particular wavelengths in a large tank. We believe that for many coastal regions the assumptions a–e and h are met as well. However, the finite size effect (f, g), and the deviation of the ocean topography from a strictly 1D case (i) could completely destroy wave localization or make it unobservable due to large uncertainties.

VII. CONCLUSION

We analyzed the problem of 1D linear potential wave propagation over an irregular topography. For simplicity, the average depth was considered to be horizontal and the irregularities (mean-square height of the irregularities) were small. Using the coordinate transformation we reduced this problem to a problem with flat boundaries and scattering in the bulk.

We developed an averaging technique, that breaks the many point correlation function into a product of lower-order correlations and the deviation from the Gaussian correlation. Using this averaging technique in combination with the Born approximation we calculated the average Green's function, the mean-free-path, the Boltzmann irreducible vertex function, the transport free path, and the problem of wave propagation over an irregular topography was mapped into the electron impurity scattering problem from solid-state physics.

The Boltzmann diffusion coefficient and the localization length for the wave energy density were expressed explicitly via the correlation function of topography, mean water depth, and wave frequency.

The dependence of the localization length on the wave number was analyzed for the random floor with the Gaussian correlation function and the random step topography. For the periodic topography (the Born approximation is not valid in this case) we recovered a trace of the first forbidden band of the Bragg resonance.

The results of the theory for the random step case were compared with some experimental results and numerical calculations. In contrast to the transfer-matrix approach, specifically designed for the 1D steplike topography, our method for small inhomogeneities is applicable to the arbitrary shape of the sea floor, and can be easily extended to a 2D case. The latter situation could include the long scale variations of

sandbars in the direction parallel to the shore line.

We discussed the limitations of the theory, such as, the limitation of the linear potential theory, wave interaction, small inhomogeneities, the Born approximation, viscous damping, finite-size effect, current, geometrically diffuse wave source, and anisotropy. The results of the theory could be verified in a tank experiment (similar to the one done by Belzons *et al.*, only with small amplitude irregularities and a much larger tank) that meets all the assumptions made in the previous section. For coastal waters a large number of assumptions made could make the localization completely impossible or very difficult to detect. However, if all of the conditions of Sec. VI are met for a certain near-shore region, particular waves are completely reflected by irregularities of the bathimetry. The observation of this phenomenon would be the first observation of a large scale Anderson localization.

ACKNOWLEDGMENTS

This work was supported in part by Professor A.E. Meyerovich, Physics Department, University of Rhode Island, NSF Grant No. DMR-9705304, and Professor C.C Mei, Department of Civil and Environmental Engineering, Massachusetts Institute of Technology, ONR Grant No. N00014-89-J-3128.

[1] A. G. Davies, Dyn. Atmos. Oceans **6**, 207 (1982).
[2] P. W. Anderson, Phys. Rev. **109**, 1492 (1958).
[3] A. Patrick Lee and T. V. Ramakrishnan, Rev. Mod. Phys. **57**, 287 (1985).
[4] J. Rammer, *Quantum Transport Theory* (Perseus, Reading, MA, 1998).
[5] J. Rammer and H. Smith, Rev. Mod. Phys. **58**, 323 (1986).
[6] D. Vollhardt and P. Wolfle, Phys. Rev. B **22**, 4666 (1980).
[7] P. Meint and Ad. Lagendijk, Phys. Rev. Lett. **55**, 2692 (1985).
[8] C. A. Condat and T. R. Kirkpatrick, *Localization of Acoustic Waves* (World Scientific, Singapore, 1990), p. 423.
[9] E. Guazzelli, E. Guyon, and B. Souillard, J. Phys. (Paris) **44**, L837 (1983).
[10] M. Belzons, E. Guazzelli, and O. Parodi, J. Fluid Mech. **186**, 539 (1988).
[11] A. E. Meyerovich and A. Stepaniants, Phys. Rev. B **58**, 13 242 (1998).
[12] A. Stepaniants, D. Sarkisov, and A. E. Meyerovich, J. Low Temp. Phys. **113**, 1159 (1999).
[13] S. M. Flatte, R. Dashen, W. S. Munk, and K. M. Watson, *Sound Transmission Through a Fluctuating Ocean* (Cambridge University Press, Cambridge, 1979).
[14] R. Dashen, J. Math. Phys. **20(5)**, 894 (1979).
[15] C. C. Mei, *The Applied Dynamics of Ocean Surface Waves* (World Scientific, Singapore, 1989).
[16] P. Sheng, *Introduction to Wave Scattering, Localization, and Mesoscopic Phenomena* (Academic Press, New York, 1995).
[17] P. Devillard, F. Dunlop, and B. Souillard, J. Fluid Mech. **186**, 521 (1988).
[18] A. Nachbin, J. Fluid Mech. **296**, 353 (1995).